Proceedings of the International School and Conference on Photonics, PHOTONICA09

Optical Properties of Y_2O_3:Eu^{3+} Red Emitting Phosphor Obtained via Spray Pyrolysis

Ž. Antić*, R. Krsmanović, V. Đorđević, T. Dramićanin and M.D. Dramićanin

Vinča Institute of Nuclear Sciences, P.O. Box 522, Belgrade, Serbia

In the present work we explored the possibility of obtaining Y_2O_3:Eu^{3+} μm-size particles by an ultrasonic spray pyrolysis method. As-prepared sample constitutes of spherical, hollow particles with an average size of 1 to 2 μm. Pure, well crystalline, cubic Y_2O_3 is formed after additional thermal treatment at 800 °C for 2 h. A detailed optical investigation has been done with photoluminescence measurements in the energy and time domains. Experimental intensity parameters, transition rates and quantum efficiency of the $^5D_0$ emission are evaluated on the basis of Judd–Ofelt theory.

PACS numbers: 32.50.+d, 81.20.Rg, 42.70.–a

1. Introduction

Spray pyrolysis is an aerosol process commonly used as a synthesis technique providing a wide variety of materials in powder form including metals, metal oxides, ceramics, superconductors and fullerenes [1, 2]. Europium-doped yttrium oxide (Y_2O_3:Eu^{3+}) is considered to be one of the best red emitting inorganic phosphors, due to the sharp emission of the europium ions at 611 nm, excellent luminescence efficiency, color purity and stability [3]. Among various synthesis procedures, spray pyrolysis is a promising alternative process for its large-scale production in a form of μm and sub-μm size spherical particles [4]. We have aimed in this work to investigate feasibility of ultrasonic spray pyrolysis (USP) method for production of Y_2O_3:Eu^{3+} powder and to calculate Eu^{3+} emission intensity parameters, transition rates and quantum efficiency in this system.

2. Results and discussion

2.1. Experimental part

A precursor solution of stoichiometric quantities of Y and Eu-nitrate was prepared by dissolving appropriate quantities of Y_2O_3 and Eu_2O_3 in hot nitric acid. In order to set total concentration in the solution to 0.5 M deionized water was added. The laboratory setup for USP consists of an ultrasonic atomizer operating at a frequency of 1.7 MHz for aerosol generation, and a horizontal electric furnace with a quartz tube and a vessel for particle collection. The working temperature was 800 °C, while the effective heating length of the reactor tube was 1 m. The flow rate of air was 30 dm^3/h. The flow rate of aerosol droplets was assumed to be equal to the flow rate of the gas carrier. The obtained material was collected in ethanol and separated from solvent using ultracentrifugation. As prepared material was dried in air and further thermally treated for 2 h at 800 °C in order to obtain pure cubic Y_2O_3 powder. X-ray diffraction (XRD) measurements were performed on the Philips PW 1050 instrument, using Ni filtered Cu $K_{\alpha 1,2}$ radiation. Diffraction data were recorded in a 2θ range from 10° to 90°, counting in 0.05° steps. Microstructure was examined with the JEOL JSM 6460LV scanning electron microscope. The photoluminescence measurements were performed at room temperature on Fluorolog-3 Model FL3-221 spectrofluorometer system (Horiba Jobin-Yvon), utilizing 450 W xenon lamp as excitation source for emission measurements and xenon–mercury pulse lamp for lifetime measurements.

2.2. XRD and SEM analysis

XRD spectra of as prepared and thermally treated powder are shown in Fig. 1. Forming of Y_2O_3 cubic phase is noticed by raising of the characteristic (222) and (044) diffraction peaks, and one can clearly see pattern originating from cubic crystalline structure of Y_2O_3 (main reflections indexed on JCPDS No. 43-0661). It can be also noticed that $Y(OH)_3$ residues are present causing reflection at 16.6°.

Scanning electron microscopy (SEM) images illustrate spherical, hollow particles, having average size of around 1 μm for as prepared sample (Fig. 1c) and around 1.2 μm for treated sample (Fig. 1d). Particles are porous and irregular that is often the case for powders derived from metal nitrates [5]. Mild temperature post-synthesis treatment caused only slight increase of the particle size as can be clearly seen from the histograms given in Fig. 2.

2.3. Emission and lifetime measurements

Emission spectrum of Y_2O_3:3at%Eu contains typical Eu^{3+} luminescence components (Fig. 3a). Five characteristic bands are associated to $^5D_0 \rightarrow {}^7F_i$ (i = 0, 1, 2, 3, 4) spin forbidden f–f transitions. As expected for the UV-VIS excitation of Eu^{3+} ions the most intense is red emission $^5D_0 \rightarrow {}^7F_2$ observed at 16377.3 cm^{-1}. It is

* corresponding author; e-mail: zeljkaa@gmail.com

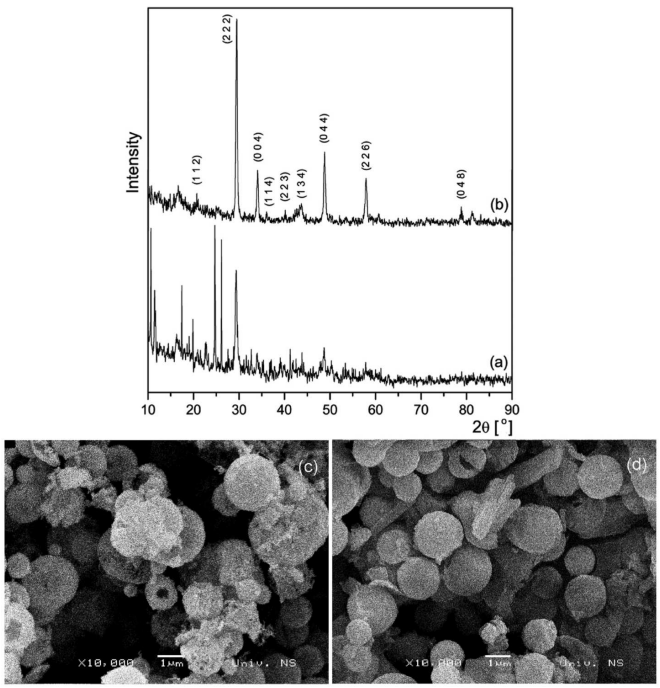

Fig. 1. XRD patterns and corresponding SEM images of: as prepared sample (a) and (d), thermally treated sample (b) and (c).

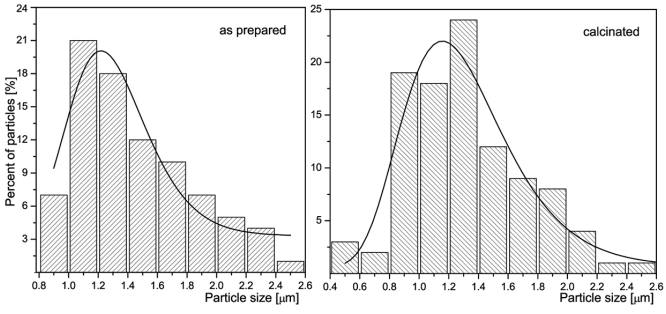

Fig. 2. Size distributions of particles in as-prepared and calcinated sample.

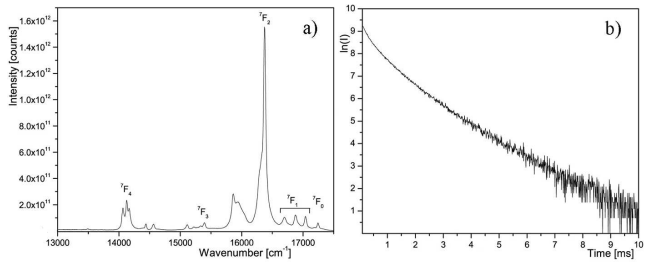

Fig. 3. Emission spectra for Y_2O_3:3at% Eu (a) and its fluorescence decay curve (b).

known that in sesquioxides emission increases with Eu^{3+} concentration increase reaching good efficiency at 3% and maximum intensity at around 5%. At higher concentration quenching of emission occurs due to exchange mechanism among the Eu^{3+} ions. The level of Eu^{3+} doping used in this work is arbitrarily chosen in a concentration range where good emission can be expected. Reduced particle size may modify emission lifetime and influence concentration quenching threshold; these effects would be subject of further work. The fluorescence decay curve presented in Fig. 3b shows that decay profile is not pure exponential, revealing more complex deexcitation path. For this reason it was more appropriate to calculate an average lifetime using following expression [6]: $\tau = \int tI(t)\,\mathrm{d}t / \int I(t)\,\mathrm{d}t$, where $I(t)$ stands for emission intensity over time, t. In this way average lifetime is calculated to be 1.1 ms.

2.4. Experimental intensity parameters, transition rates and quantum efficiency of the $^5D_0$ emission

The spectra of trivalent lanthanide in solution or crystal lattice arise from forbidden transitions within the $4f^n$-configuration to which the Judd–Ofelt (JO) [7, 8] theory has been successfully applied in quantitative determination of its optical properties. The application of JO theory to the quantitative analysis of Eu^{3+} emissive properties in matrix is nicely presented by Werts et al. [9], and can be summarized as follows.

Radiative relaxation from an excited state ΨJ of a lanthanide ion usually occurs to various lower lying states $\Psi' J'$, giving rise to several lines in the emission spectrum. The red luminescence of Eu^{3+} is a result of transitions from its $^5D_0$ state to all of the lower lying ^7F_J levels. According to JO theory the spontaneous emission probability, A, of the transition $\Psi J \rightarrow \Psi' J'$ is related to its dipole strength according to the following equation:

$$A(\Psi J, \Psi' J') = \frac{64\pi^4 \nu_{\mathrm{avg}}^4}{3h(2J+1)} \times \left[\frac{n(N^2+2)^2}{9} D_{\mathrm{ED}} + n^3 D_{\mathrm{MD}}\right], \quad (1)$$

where ν_{avg} is the average transition energy in cm^{-1}, h is Planck constant (6.63×10^{-27} erg s), $2J+1$ is the degeneracy of the initial state (1 for $^5D_0$). D_{ED} and D_{MD} are the electric and magnetic dipole strength (in $\mathrm{esu}^2\ \mathrm{cm}^2$), respectively. The factors containing medium's refractive index n result from local field corrections that convert the external electromagnetic field into an effective field at the location of the active center in the dielectric medium.

The transitions from $^5D_0$ to $^7F_{0,3,5}$ are forbidden both in magnetic and induced electric dipole schemes (D_{ED} and D_{MD} are zero). The transition to $^7F_1$ ($J' = 1$) is the only magnetic dipole transition, and has no electric dipole contribution. Magnetic dipole transitions in lanthanide ions are practically independent of the ion's surroundings, and can be well calculated by theory ($D_{\mathrm{MD}} = 9.6 \times 10^{-42}\ \mathrm{esu}^2\ \mathrm{cm}^2 = 9.6 \times 10^{-6}\ \mathrm{D}^2$) [10].

The remaining transitions ($J' = 2, 4, 6$) are purely of induced electric dipole nature, and the strength of

all induced dipole transitions can be calculated on basis of only three phenomenological parameters Ω_λ (JO parameters) using the following equation:

$$D_{\mathrm{ED}} = e^2 \sum_{\lambda=2,4,6} \Omega_\lambda \left| \langle \Psi J \| U^{(\lambda)} \| \Psi' J' \rangle \right|^2, \quad (2)$$

where e stands for elementary charge e and $|\langle \Psi J \| U^{(\lambda)} \| \Psi' J' \rangle|^2$ are the squared reduced matrix elements whose values are independent of the chemical environment of the ion. For the case of Eu^{3+} these values are given in Refs. [11, 12].

In case of Eu^{3+} each electric dipolar $^5D_0 \rightarrow {}^7F_{2,4,6}$ transition depends only on one squared reduced matrix element. This unique feature for the Eu^{3+} ion facilitates the determination of JO parameters from the emission spectra. Thus, the experimental intensity Ω_λ can be calculated from the ratio of the intensity of the $^5D \rightarrow {}^7F_\lambda$ ($\lambda = 2$, 4 and 6) transitions, $\int I_\lambda(\nu)\,\mathrm{d}\nu$, to the intensity of the $^5D \rightarrow {}^7F_1$ transition $\int I_1(\nu)\,\mathrm{d}\nu$, as follows:

$$\Omega_\lambda = \frac{D_{\mathrm{MD}}\nu_1^3}{e^2\nu_\lambda^3} \frac{9n^3}{n(n^2+2)^2 \left| \langle \Psi J \| U^{(\lambda)} \| \Psi' J' \rangle \right|^2} \times \frac{\int I_\lambda(\nu)\,\mathrm{d}\nu}{\int I_1(\nu)\,\mathrm{d}\nu}. \quad (3)$$

Then, probabilities of each spontaneous emission (radiative rates) can be obtained from Eqs. (1) and (2) using calculated Ω_λ parameters. Total radiative rate, A_{R}, defined as sum of all radiative rates, can be further used to evaluate nonradiative rate, A_{NR}, and emission quantum efficiency, η (ratio between number of photons emitted by the Eu^{3+} ion to those absorbed by the Eu^{3+} ion) in the following way:

$$A_{\mathrm{NR}} = 1/\tau - A_{\mathrm{R}}, \quad \eta = A_{\mathrm{R}}/\left(A_{\mathrm{R}} + A_{\mathrm{NR}}\right), \quad (4)$$

where τ stands for the emission lifetime.

Results of calculation are given in Table. In the present work Ω_6 has been neglected since this parameter is considerably smaller in comparison to Ω_2 and Ω_4 [13].

TABLE

$\Omega_{2,4}$ parameters, radiative transition rates, nonradiative rate, experimental lifetime and emission quantum efficiency of Y_2O_3:Eu^{3+}.

Ω_2	Ω_4	A_1	A_2	A_4	A_{R}	A_{NR}	τ	η
$[10^{-20}$ cm$^2]$		$[s^{-1}]$					[ms]	[%]
9.9	3.6	102.3	630.9	102.6	835.8	73.3	1.1	91.9

It is worth noting that values of the intensity parameters, Ω_2 and Ω_4, and radiative rate are much higher compared to those reported for Eu^{3+} in Y_2O_3 [14, 15] and comparable to values obtained when this material is codoped with Al^{3+} and B^{3+} [15].

3. Conclusion

By taking into account observed structural, morphological and radiative properties of obtained Y_2O_3 phosphor powder, and especially very high value of emission quantum efficiency ($\approx 92\%$), one can conclude that this material possesses favorable properties for applications as red phosphor in optoelectronic devices, in particular for luminescent displays.

Acknowledgments

Authors acknowledge the financial support of the Ministry of Science of the Republic of Serbia (project 141026). R. Krsmanović is thankful to the NATO financial support (grant reference number CBP.EAP.RIG.983373).

References

[1] A. Gurav, T. Kodas, T. Pluym, Y. Xiong, *Aerosol Sci. Technol.* **19**, 411 (1993).

[2] S.E. Pratsinis, S. Vemury, *Powder Technol.* **88**, 267 (1996).

[3] C.R. Ronda, *J. Lumin.* **72-74**, 49 (1997).

[4] Y.C. Kang, S.B. Park, I.W. Lenggoro, K. Okuyama, *J. Mater. Res.* **14**, 2611 (1999).

[5] G.L. Messing, S.-C. Zhang, G.V. Jayanthi, *J. Am. Ceram. Soc.* **11**, 2707 (1993).

[6] E. Nakazawa, *Phosphor Handbook*, CRC Press, Boca Raton FL 1999.

[7] B.R. Judd, *Phys. Rev.* **127**, 750 (1962).

[8] G.S. Ofelt, *J. Chem. Phys.* **37**, 511 (1962).

[9] M.H.V. Werts, R.T.F. Jukes, J.W. Verhoeven, *Phys. Chem. Chem. Phys.* **4**, 1542 (2002).

[10] M.J. Weber, T.E. Varitimos, B.H. Matsinger, *Phys. Rev. B* **8**, 47 (1973).

[11] W.T. Carnall, H. Crosswhite, H.M. Crosswhite, *Energy Level Structure and Transition Probabilities of the Trivalent Lanthanides in LaF_3*, Argonne National Laboratory, Argonne IL 1977.

[12] W.T. Camall, P.R. Fields, K. Rajnak, *J. Chem. Phys.* **49**, 4450 (1968).

[13] R. Balakrishnaiah, R. Vijaya, P. Babu, C.K. Jayasankar, M.L.P. Reddy, *J. Non-Cryst. Solids* **353**, 1397 (2007).

[14] Q. Lü, A. Li, F. YunGuo, L. Sun, L. Zhao, *Nanotechnology* **19**, 205704 (2008).

[15] R. Debnath, A. Nayak, A. Ghosh, *Chem. Phys. Lett.* **444**, 324 (2007).